3-D electrical resistivity structure based on geomagnetic transfer functions exploring the features of arc magmatism

Maki HATA[1] and Makoto UYESHIMA[2]
[1]National Institute of Advanced Industrial Science and Technology, Central 7, Higashi 1-1-1, Tsukuba, Ibaraki 305-8567, Japan
[2]Earthquake Research Institute, the University of Tokyo, Yayoi 1-1-1, Bunkyo-ku, Tokyo 113-0032, Japan

SUMMARY

Our 3-D electrical resistivity model show volcanism/magmatism associated with subduction of the Philippine Sea Plate (PSP) in three regions: a southern and a northern volcanic region, and a nonvolcanic region on the island of Kyushu, SW Japan. By setting a previous 3-D model, which was obtained by Network-Magnetotelluric (MT) response function data of a longer-period band (480−40,960 s), as an initial model, we inverted geomagnetic transfer function data of a short-period band (20−960 s). We aimed at enhancing model resolutions at shallower depths in this study. In order to examine the model resolution enhancement, we performed sensitivity tests to compare respective model resolutions by using actual measurement configurations (such as the spatial distribution of observation sites and sets of data periods) for the geomagnetic and the Network-MT data. Checkerboard patterns at shallower depths were more clearly recovered using the measurement configuration of the geomagnetic data than when using the configuration of the Network-MT data. Finally, in addition to characteristics of the previous model, the present model reveals a conductive block on the back-arc side of Kirishima volcano at shallow depths of ~50 km; the block is associated with hydrothermal fluids and hydrothermal alteration zones related to the formation of epithermal gold deposits in the Hisatsu and Hokusatsu zones.

Keywords: Arc magmatism, geomagnetic transfer function, Network-Magnetotelluric response function, Comparative verification of model resolutions, 3-D electrical resistivity imaging

INTRODUCTION

Observations of geomagnetic variations in Japan have been used to investigate subsurface electrical resistivity structures associated with subduction systems since the 1950s [e.g., *Rikitake*, 1969]. For graphical representations of geomagnetic variations, induction vector analysis [*Parkinson*, 1962] is widely used, as the induction vector (arrow) in the Parkinson convection points to an area of electric current concentration associated with a conductive anomaly. Induction arrows on the Japan Islands generally point to the Pacific Ocean of deep-sea in a large sense [e.g., *Yukutake et al.*, 1983]. However, induction arrows in northern and central Kyushu point to the relatively shallow East China Sea [e.g., *Handa et al.*, 1992], rather than to the Pacific Ocean. In southern Kyushu, induction arrows derived from short-period (less than several hundred seconds) data on the western and eastern coasts point to the East China Sea and the Pacific Ocean, respectively, whereas arrows of long-period (greater than several hundred seconds) data are oriented parallel to the coastline [e.g., *Shimoizumi et al.*, 1997; *Munekane*, 2000]. The complex behavior of the induction arrows observed on Kyushu is considered to result from the complex subsurface electrical resistivity structures due to e.g., subduction related arc magmatism (Fig. 1).

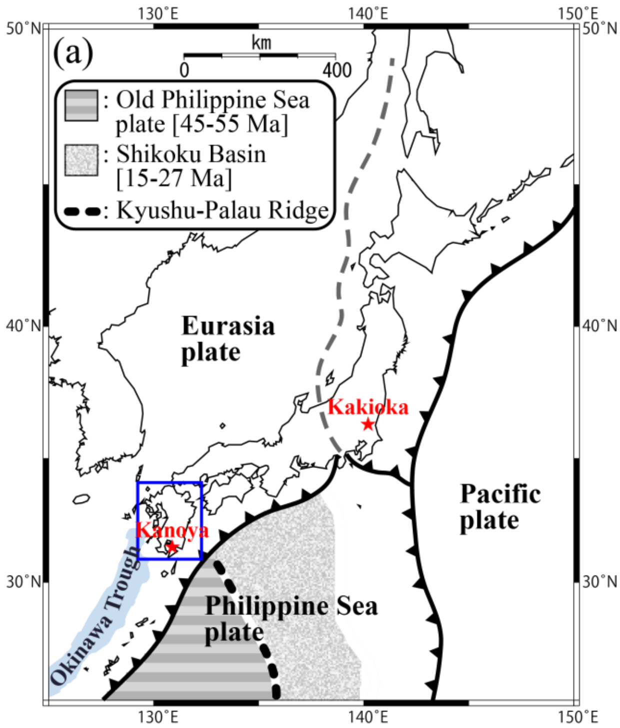

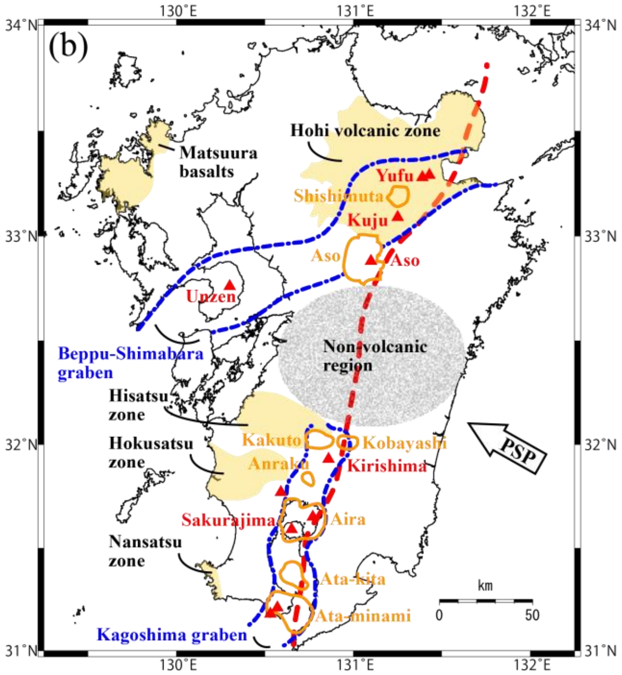

Figure 1. (a) Locations of plate boundaries in the Japan arc (toothed lines). Red stars represent the Kakioka and Kanoya Magnetic Observatories (JMA), whose magnetic data were used as areference and a remote-reference. A blue box represents the range of Fig. 1b. **(b)** The tectonic setting around the Kyushu Island is characterized by active Quaternary volcanoes (red triangles), calderas (orange rings), two grabens (blue dashed lines), lava plateaus (pale orange shaded regions), and a volcanic front (red dashed line). The arrow labeled 'PSP' indicates the subduction direction of the Philippine Sea Plate. The figure is taken from *Hata et al.* [2016].

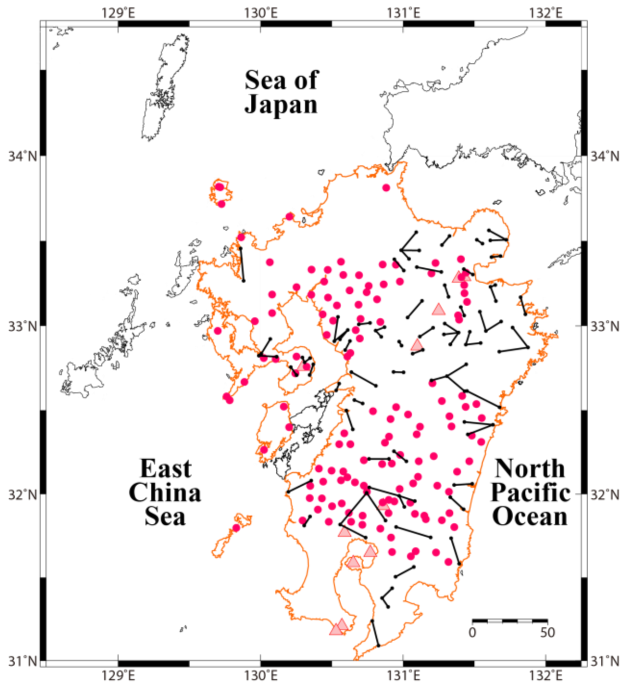

Figure 2. Spatial distribution of geomagnetic observation sites (red dots) and Network-MT observation sites (black lines). The black lines denote dipoles used to obtain electrical potential difference values. Pink triangles indicate active Quaternary volcanoes. The 136 geomagnetic sites and the 72 Network-MT dipoles, located on the main Kyushu Island and the three small islands (region outlined in orange), were used in the 3-D inversions.

3D INVERSE MODELING

Geomagnetic transfer function (TF) data were introduced to improve the resolution at crustal depths of an electrical resistivity structure model obtained previously using only Network-MT data (black lines in Fig. 2) [*Hata et al.*, 2015]. Observed three-component geomagnetic variations are converted to TFs, expressed as $Hz(\mathbf{r}, T) = A(\mathbf{r}, T)\, Hx(\mathbf{r}, T) + B(\mathbf{r}, T)\, Hy(\mathbf{r}, T)$, where $Hz(\mathbf{r}, T)$ is the vertical geomagnetic field, $Hx(\mathbf{r}, T)$ and $Hy(\mathbf{r}, T)$ are the horizontal components of the geomagnetic field, $\mathbf{r}$ is the location of observation sites, and T is the period. The geomagnetic TFs $A(\mathbf{r}, T)$ and $B(\mathbf{r}, T)$ are complex values. The electrical resistivity structure is determined using the two TFs of $A(\mathbf{r}, T)$ and $B(\mathbf{r}, T)$, which are sensitive to the distribution of the gradient of electrical conductivity [e.g., *Rikitake and Yokoyama*, 1953]. To obtain the 3-D electrical resistivity structure beneath the whole Kyushu Island, we utilized data from 136 sites on the main Kyushu Island and three small islands, as shown in Fig. 2 (red dots in orange outlined islands).

Sensitivity Tests for Comparative Verification of Model Resolutions

The goal of this study was to obtain a 3-D electrical resistivity model at shallow depths with a resolution higher than that of previous 2-D and 3-D models, which were obtained solely by the Network-MT RFs [e.g., *Hata et al.*, 2015], by introducing geomagnetic TFs. We performed sensitivity tests to compare respective model resolutions by using actual measurement configurations (such as the spatial distribution of observation sites and sets of data periods) for the geomagnetic and the Network-MT data. Eight inversions were performed using synthetic data, to which a 5% Gaussian noise was added to estimate the model resolution; this was accomplished using four checkerboard patterns in Fig. 3a−d. Four of the eight inversions, (a′)−(d′), were performed using the geomagnetic data configuration, whereas the other four inversions, (a″)−(d″), were performed using the Network-MT data configuration. In addition, the conductive and resistive blocks are interchangeable between (a)−(b) and (c)−(d). The conductive and resistive blocks of the checkerboard patterns were more clearly recovered using the measurement configuration of the geomagnetic data (Fig.

3a′ and b′) than when using the configuration of the Network-MT data (Fig. 3a″ and b″).

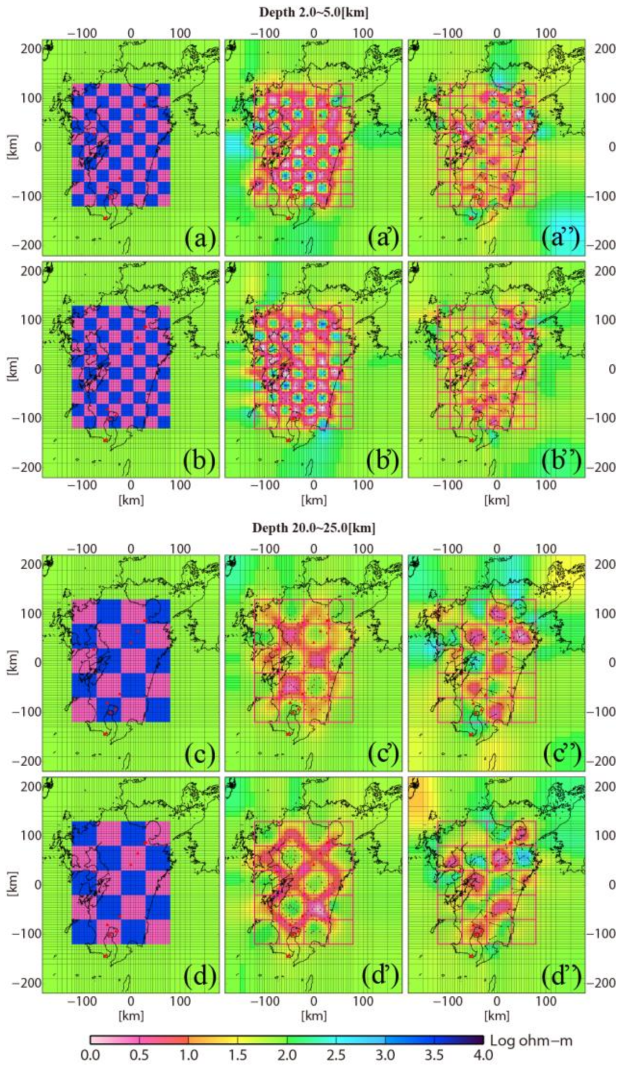

Figure 3. Plan views of four checkerboard patterns, (a)−(d), used in resolution tests in this study, and views of eight resolution test models, (a′)−(d′), obtained using the actual measurement configuration provided by the 136 geomagnetic TFs, (a″)−(d″), obtained using the configuration of the 72 Network-MT RFs. The four checkerboards, (a)−(d), were used to obtain the synthetic data, to which 5% Gaussian noise was added before the inversion. Patterns (a) and (c) are opposite those of (b) and (d), respectively. The resistivity values of the conductive and resistive blocks in all checkerboard patterns are 3 Ωm and 3000 Ωm, respectively. All checkerboard patterns have dimensions of 250 × 200 km in the X and Y directions. The patterns of (a) and (b), and those of (c) and (d), consist of 80 blocks (25 × 25 km alternately in the horizontal direction) and 20 blocks (50 × 50 km alternately in the horizontal direction), respectively. The thicknesses of inserted checkerboard patterns are set to 0–10 km [(a) and (b)] and 10–40 km [(c) and (d)] in the vertical direction. Eight plan-view sections, (a′)−(d′) and (a″)−(d″), of the inverted models show sections 2–5 km in depth [(a′), (b′), (a″), and (b″)] and 20–25 km in depth [(c′), (d′), (c″), and (d″)]. Volcanoes (red triangles) are shown in each section, while the 136 geomagnetic observation sites (red dots) are shown in the four sections (a′)−(d′), and the 72 dipoles (black lines with endpoints) are shown in the other four sections, (a″)−(d″).

CONCLUDING REMARKS

The well-determined electrical resistivity model beneath the island of Kyushu, based on a previous large-scale model [*Hata et al.*, 2015], was obtained through a 3-D inversion analysis by introducing geomagnetic TFs as additional input data. As expected from the resolution tests, the final 3-D model using the actual measurement configuration of the geomagnetic data shows higher resolutions, especially for small-scale structures at shallow depths, than the previous model. This result shows improved resolution at crustal depth using different data sets, without any joint inversion.

In addition to characteristics of the previous model, the present model reveals a conductive block on the back-arc side of Kirishima volcano at shallow depths of ~50 km; the block is associated with hydrothermal fluids and hydrothermal alteration zones related to the formation of epithermal gold deposits in the Hisatsu and Hokusatsu zones.

ACKNOWLEDGMENTS

We thank W. Siripunvaraporn and coworkers for providing the WSINV3DMT code. We also thank A.D Chave and D.J. Thomson for providing their robust remote-reference magnetotelluric (BIRRP) code. We used the computer systems of the Earthquake Information Center of the Earthquake Research Institute, University of Tokyo.

REFERENCES

Chave, A.D., and Thomson, D.J., 2004, Bounded influence magnetotelluric response function estimation, *Geophys. J. Int.*, **157**, 988–1006.

Handa, S., Tanaka, Y., and Suzuki, A., 1992, The electrical high conductivity layer beneath the northern Okinawa Trough, inferred from geomagnetic depth sounding in Northern and Central Kyushu, Japan, *J. Geomag. Geoelectr.*, **44**, 505–520.

Hata, M., Oshiman, N., Yoshimura, R., Tanaka, T., and Uyeshima, M., 2015, Three-dimensional electromagnetic imaging of upwelling fluids in the Kyushu subduction zone, Japan, *J. Geophys. Res.*, **120**, doi: 10.1002/2014JB011336.

Hata, M., Uyeshima, M., Handa, S., Shimoizumi, M., Tanaka, Y., Hashimoto, T., Kagiyama, T., Utada, H., Munekane, H., Ichiki, M., and Fuji-ta, K., 2016, 3-D electrical resistivity structure based on geomagnetic transfer functions exploring the features of arc magmatism beneath Kyushu, Southwest Japan Arc, *J. Geophys. Res. Solid Earth*, **122**, doi:10.1002/2016JB013179.

Munekane, H., Kagiyama, T., Utada, H., Kanda, W., Matsutani, F., Koyama, S., Amita, K., Oba, S., Mishina, M., Yamamoto, T., Yamazaki, A., Kato, W., and Umeda, K., 1997, Resistivity Survey Across the Southern Part of the Kyushu Island, *Bull Earthq. Res. Inst. Univ. Tokyo*, **72**, 19–65, (in Japanese with English abstract).

Parkinson, W.D., 1962, The Influence of Continents and Oceans on Geomagnetic Variations, *Geophys. J. Int.*, **6**, 441–449.

Rikitake, T., and Yokoyama, I., 1953, Anomalous relations between H and Z components of transient geomagnetic variations, *J. Geomag. Geoelectr.*, **5**, 59–65.

Rikitake, T., 1969, The undulation of an electrically conductive layer beneath the islands of Japan, *Tectonophysics*, **7**, 257–264.

Shimoizumi, M., Mogi, T., Nakada, M., Yukutake, T., Handa, S., Tanaka, Y., and Utada, H., 1997, Electrical conductivity anomalies beneath the western sea of Kyushu, Japan, *Geophys. Res. Lett.*, **24**, 1551–1554.

Siripunvaraporn, W., and Egbert, G., 2009, WSINV3DMT: Vertical Magnetic Field Transfer Function Inversion and Parallel Implementation, *Physics of the Earth and Planetary Interiors*, **173(3-4)**, 317–329.

Yukutake, T., Filloux, J.H., Segawa, J., Hamano, Y., and Utada, H., 1983, Preliminary Report on a Magnetotelluric Array Study in the Norhtwest Pacific, *J. Geomag. Geoelectr.*, **35**, 575–587.